Single fundamental mode photonic crystal VCSEL with high power and low threshold current optimized by modal loss analysis*

Yi-Yang Xie(解意洋)[1,2], Qiang Kan(阚强)[2], Chen Xu(徐晨)[1,†], Kun Xu(许坤)[3], and Hong-Da Chen(陈弘达)[2]

[1] *Key Laboratory of Optoelectronics Technology (Ministry of Education), Beijing University of Technology, Beijing* 100124, *China*
[2] *State Key Laboratory of Integrated Optoelectronics, Institute of Semiconductor, Chinese Academy of Sciences, Beijing* 100083, *China*
[3] *Zhengzhou University of Aeronautics, Zhengzhou* 450046, *China*

(Received 9 May 2016; revised manuscript received 18 September 2016; published online 30 November 2016)

The characteristics of the photonic crystal vertical cavity surface emitting lasers (PhC-VCSELs) were investigated by using the full vector finite-difference time-domain (FDTD) method through the transverse mode loss analysis. PhC-VCSELs with different photonic crystal structures were analyzed theoretically and experimentally. Through combining the dual mode confinement of oxide aperture and seven-point-defect photonic crystal structure, the PhC-VCSELs with low threshold current of 0.9 mA and maximum output power of 3.1 mW operating in single fundamental mode were demonstrated. Mode loss analysis method was proven as a reliable and useful way to analyze and optimize the PhC-VCSELs.

Keywords: vertical cavity surface emitting lasers, single fundamental mode, mode loss

PACS: 42.55.Px, 42.55.Tv, 42.62.Fi **DOI:** 10.1088/1674-1056/26/1/014203

1. Introduction

Single-fundamental-mode (SFM) vertical cavity surface emitting lasers (VCSELs) are necessary for a number of applications, including high-speed laser printing, optical storage, and longer-wavelength telecommunications.[1–8] Therefore, various methods were proposed and demonstrated to obtain SFM-VCSELs. As described in the literature, SFM-VCSEL has been fabricated mainly using two different techniques. One technique is to make the device waveguide narrow and the effective index step sufficiently small to only support the fundamental (LP_{01}) mode.[1–3] The small oxide aperture confined VCSEL can operate in single fundamental mode due to the narrow waveguide structure, while it suffers from high electric resistance as a result of the small current injection area.[2,3] The high electric resistance is not acceptable for high speed modulation. Moreover, the small oxide aperture cannot achieve high output power. The other technique is introducing a mode-selective loss structure in the inherently multimode VCSELs to inhibit high-order transverse modes emission.[4–11] Metal aperture, anti-resonant reflecting element, surface-relief etching, hybrid oxide-implant VCSELs, extended cavity, holey structure, and defected photonic crystal air-hole array can introduce larger loss for the high-order transverse modes. Among these methods, the photonic crystal has been demonstrated to be a reliable way for transverse mode control because of a suitable refractive index which can be adjusted by the variety of the photonic crystal parameters, such as air-hole depths, diameters, and arrangement.[11–26] With a proper selection of these parameters, VCSELs can easily work with high single fundamental mode output power,[10,11] high modulation speed,[12] and small divergence angle.[13,14] The best PhC-VCSEL results reported to date include output power over 3 mW,[11,23] far-field divergence angle less than 6°,[24] and a modulation bandwidth over 10 GHz.[12] Polarization stable SFM PhC-VCSEL has also been demonstrated.[17,25]

In PhC-VCSELs, the photonic crystal structure is the dissipation element for the high-order transverse modes due to the scattering loss of the photonic crystal air holes. As a result, only the fundamental mode will lase through the light emission aperture. So the transverse mode loss analysis is very important for the PhC-VCSELs. Most of the previous reported simulations treat the PhC-VCSELs as a 2D or quasi-3D structure.[12–16] Many of the analyses are based on the photonic crystal fiber model, which can be used to match the experimental data. When the transverse modes are not affected by the oxide aperture (the oxide aperture diameter is large enough), the photonic crystal fiber model can be used to optimize the parameters of PhC-VCSELs. However, these oversimplified approaches are difficult for analyzing the loss of various transverse modes precisely and optimizing all of the VCSEL structure parameters. Alias *et al.* proposed a new semi-empirical method to analyze the single mode condition

*Project supported by the National Basic Research Program of China (Grant Nos. 2010CB934104, 2009CB320300, and 2011CBA00608) and the National Natural Foundation of China (Grant Nos. 61604007, 61378058, 61376049, 61575008, and 61574011).

†Corresponding author. E-mail: xuchen58@bjut.edu.cn

© 2017 Chinese Physical Society and IOP Publishing Ltd

and calculate the loss as a function of the mode order based on the finite difference frequency domain (FDFD) method.[27,28] Recently, the full-vector three-dimensional (3D) FDTD was used to analyze the quality factors of varies transverse modes, which correspond to the mode loss.[26,29,30] The 3D FDTD simulation is a simple and straightforward algorithm for solving time-dependent electromagnetic problems. The algorithm requires minimal assumptions and approximations and provides fairly reliable results.[26,29,30]

In this paper, the loss analysis of transverse modes was utilized for optimized PhC-VCSELs using the full vector 3D FDTD method without any simplification and assumption to obtain the high output power, low threshold current, single fundamental mode PhC-VCSELs. The mode losses affected by the photonic crystal parameters were analyzed in detail. PhC-VCSELs with single-point-defect and seven-point-defect were analyzed theoretically and experimentally, and the analysis results illustrated the reason of the seven-point-defect PhC-VCSELs performing better than the single-defect one. More importantly, the transverse modes loss affected by the oxide aperture diameter was also analyzed to obtain sufficient loss for high order modes and less loss for the fundamental mode. Through combining the two types of mode-confined mechanisms, by both the photonic crystal and the oxide aperture, high single fundamental mode output power PhC-VCSELs were demonstrated operating at low threshold current.

2. Design and experiment

The threshold current $I_{\rm th}$ of the oxide-confined PhC-VCSELs can be obtained from the rate equations and expressed by the followed equation:[2,31,32]

$$I_{\rm th} = eB_{\rm eff}\frac{V_{\rm a}}{\eta_{\rm i}\eta_{\rm spon}}\left(N_{\rm t} + \frac{1}{(c/n_{\rm eq})({\rm d}g/{\rm d}N)}\frac{1}{\xi}\frac{1}{\tau_{\rm p}}\right)^2, \quad (1)$$

where N is the carrier density, Γ is the confinement factor of the lasing mode, g is the optical gain per centimeter, $N_{\rm t}$ is the transparent carrier density, c is the velocity of light, $V_{\rm a}$ is the volume of the active region, which is given by $V_{\rm a} = \pi\,(D/2)^2 h$, h is the total active layer thickness, D is the diameter of the oxide aperture, e is the electron charge, $J_{\rm th}$ is the threshold current density, and $B_{\rm eff}$ is the effective recombination coefficient. $\tau_{\rm p}$ is the photon lifetime in the cavity, which is given by

$$\tau_{\rm p} = n_{\rm eq}/c(\alpha_{\rm a} + \alpha_{\rm d} + \alpha_{\rm m}), \quad (2)$$

where $\alpha_{\rm a}$ is the absorption loss, $\alpha_{\rm d}$ is the diffraction loss, and $\alpha_{\rm m}$ is the mirror loss coefficient

$$\alpha_{\rm m} = \frac{1}{L}\ln\left(\frac{1}{R_{\rm top}\times R_{\rm down}}\right), \quad (3)$$

with L being the cavity length, and $R_{\rm top}$ and $R_{\rm down}$ being the top and the bottom DBRs reflectance of the VCSEL. The mirror mode loss in the devices was determined by the top reflector reflectance because the reflectance of the bottom reflector was 1. Therefore, controlling the mirror mode loss can effectively reduce the threshold current. In the PC-VCSEL, the SFM was obtained by introducing different mirror mode loss of the cavity mode. Therefore, optimization of the mode loss, which was introduced by the PC structure, can obtain the device with high power and low threshold current.

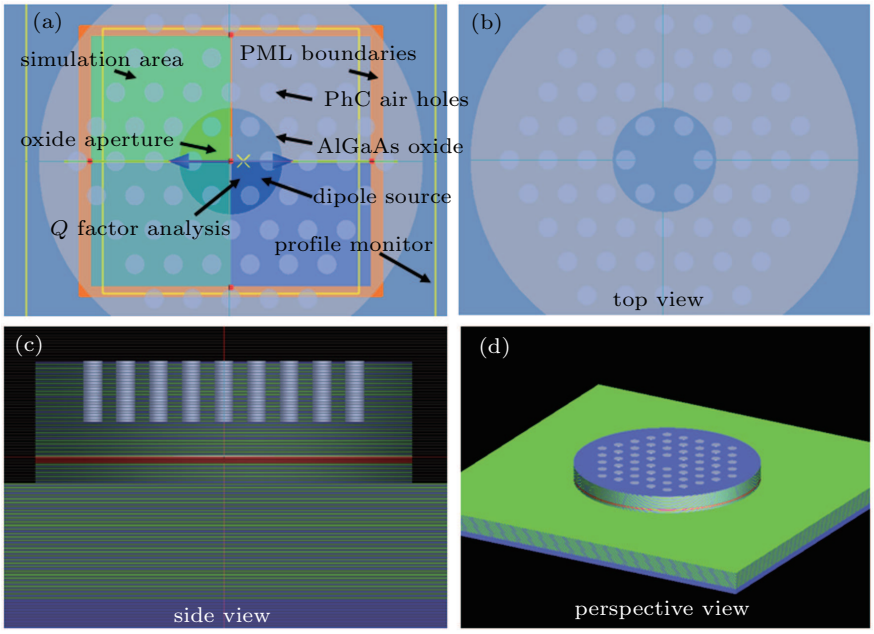


Fig. 1. (color online) (a) PhC-VCSELs model and (b)–(d) various views of the model in FDTD.

In order to analyze the mode characteristics of the PhC-VCSELs, the Lumerical's FDTD solution was used to analyze the PhC-VCSELs. Figure 1 shows a schematic of the simulated PhC-VCSEL. An oxide layer with a circular aperture was located between the active layer and the top distributed Bragg reflector (DBR).[26,29,33–37] The refractive index of every layer in the VCSEL structure was needed for the full 3D FDTD model, which was obtained from Refs. [38] and [39] and listed in Table 1.

Table 1. Details of the layer structure of the analyzed PhC-VCSELs.

Layer	Thickness/nm	Material	Refractive index (850 nm)
		air	1.0
Top DBR	59	Al(0.12)GaAs	3.52
22.5 pairs	70	Al(0.9)GaAs	3.11
Oxide layer	30	Al(0.98)GaAs/Al2O3	3.08/1.6
	30.5	Al(0.9)GaAs	3.11
Cavity	107	Al(0.3)GaAs	3.40
	3×6+2×8	GaAs/Al(0.3)GaAs	3.62/3.40
	107	Al(0.3)GaAs	3.40
Bottom DBR	59	Al(0.12)GaAs	3.52
34.5 pairs	70	Al(0.9)GaAs	3.11
Substrate		GaAs	3.62

In the FDTD simulation, the boundary conditions were set by adding a perfectly matched layer (PML) around the computational domain of the VCSEL structure to absorb any outgoing waves. The spatial resolution, or the dimensions of the grids, determined the computation time and the accuracy of finite difference approximations. We used the optimal resolutions that yielded reliable accuracy with reasonable computation time, which are $\Delta x = \Delta y = 0.15$ μm and $\Delta z = 0.015$ μm in our VCSEL structure (Δx, Δy, and Δz are the unit grid size). The small grid size along the z axis was selected because light propagated along the z axis with both the optical phase and the amplitude of the laser modes varying fast. A single dipole source was used to generate optical waves and excite multiple resonant modes. The Q factor of all of the modes was used to analyze the mode loss and optimize the structure parameters of the PhC-VCSELs. The cavity mode field distribution of the resonant modes was also used in the model to analyze the scattering loss.

The PhC-VCSELs were fabricated with the following process flow. A VCSEL epitaxial structure with 850-nm emission wavelength was grown on an n-GaAs substrate. The material contained 22.5-pairs of p-type top DBR and 34.5-pairs of n-type bottom DBR, consisting of alternating $Al_{0.9}Ga_{0.1}As/Al_{0.12}Ga_{0.88}As$ layers. A 30 nm $Al_{0.98}Ga_{0.02}As$ oxidation layer was included in the top DBR above the active region. The circular mesa was formed by $SiCl_4/Ar/Cl_2$ inductively coupled plasma reaction ion etching (ICP-RIE) down to the active region with SiO_2 etch mask. The $Al_{0.98}Ga_{0.02}As$ layer was then selectively oxidized forming the 8 μm, 9 μm, 10.5 μm, and 12 μm current confinement apertures. Afterward the top ohmic (Ti/Au) ring contacts were patterned, and the bottom ohmic (Au/Ge/Ni/Au) contacts formed and annealed using rapid thermal annealing at 430 °C for 35 s. The photonic crystal holes were then patterned using electron beam lithography and transferred into the top DBR using $SiCl_4/Ar/Cl_2$ ICP-RIE, the etching conditions were optimized for minimizing the surface etching damage. For the photonic crystal structure, a moderate b/a ratio 0.5 was selected in our experiment to minimize the optical field leakage resulting from narrower air holes and the diffraction losses caused by wider air holes.[13–26,33–37] The seven-point-defect and another three single-point-defect photonic crystal structures were selected and arranged in the same chip. The detailed parameters of the devices are shown in Table 2 and the scanning electron microscope images of the devices are shown in Fig. 2.

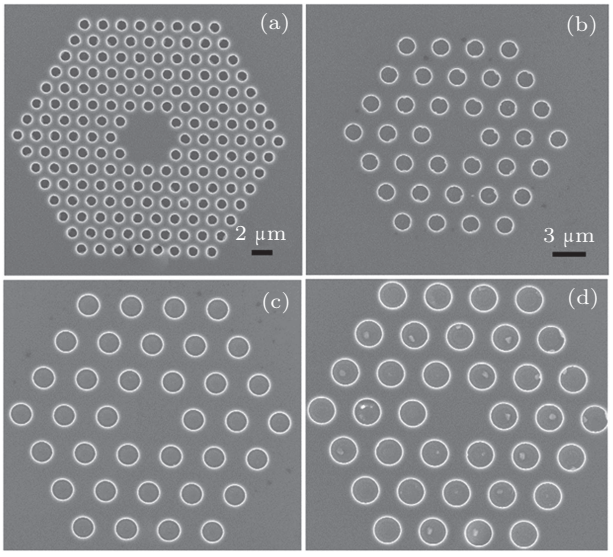


Fig. 2. The SEM image of the fabricated PhC-VCSELs: (a) type 1, (b) type 2, (c) type 3, (d) type 4.

Table 2. Detailed parameters of the fabricated PhC-VCSELs.

Type	Lattice constant/μm	Air hole diameter/μm	Number of point defects	Etching depth/μm	Central defect diameter/μm
1	2	1	7	1.8	7
2	3	1.5	1	1.9	4.5
3	5	2.5	1	2.2	7.5
4	5	3	1	2.5	7

3. Results and discussion

The device measurement was performed at room-temperature (RT) under continuous-wave (CW) operation. The light output power versus current (L–I) characteristics were measured with precise variation of the input current (using a semiconductor parameter analyzer). The light output power was detected by a silicon photodetector which was also connected to the semiconductor parameter analyzer. The beam profile of the device was obtained using a goniometric ra-

diometer far-field detector positioned on the far point of a rotating mechanical arm. Far-field angular divergences were obtained by the arm rotating. The output spectrum of VCSEL was obtained by coupling the laser beam into an optical fiber connected to an Agilent 8614xB optical spectrum analyzer.

3.1. Mode loss analysis with different photonic crystal structure

Here four types of PhC-VCSELs shown in Table 2 were fabricated and tested. Figure 3 shows the typical RTCW *L–I* characteristics of the produced PhC-VCSELs with 8-μm oxide aperture diameter and different photonic crystal structure parameters. All of the devices were formed on one chip with the same fabrication process. The maximum output power of the type 1 PhC-VCSELs is 1.7 mW and the threshold current of the devices is less than 1 mA. The slope efficiency of the device is 0.233 W/A. The maximum output power of the type 2 PhC-VCSELs is 1.05 mW and the threshold current is 2.8 mA. The slope efficiency of the type 2 device is 0.103 W/A. The maximum output power of the type 3 and type 4 PhC-VCSELs is higher than 2 mW and the threshold current is less than 1 mA. The slope efficiency of the type 3 and type 4 devices is higher than 0.3 W/A. From the experimental results of the type 1 and type 2 devices, we can find that the output power of the devices is dependent on the central defect diameter of the PhC-VCSELs. Therefore, enlarging the central defect diameter is essential to improve the output power of the devices.

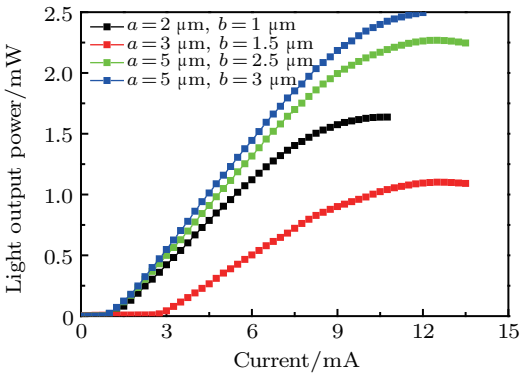


Fig. 3. (color online) The *L–I* of the fabricated PhC-VCSELs measured at room temperature.

Figure 4 shows the far-field distributions of the devices measured at the maximum output power. The type 1 and type 2 devices' divergence angles are less than 10° and the far-field distribution is of one intensity peak, illustrating single transverse mode operating and the improved beam quality by introducing the photonic crystal on the top DBR. The type 3 and type 4 devices' divergence angles are more than 10° and the beam profiles have multiple intensity peaks, which reveal that the laser operates in multi-transverse modes.[14,24]

Figure 5 shows the optical spectra of the fabricated PhC-VCSELs. The spectral full widths at half maximum (FWHMs) of the type 1 and type 2 devices are less than 0.1 nm (limited by the resolution of the optical spectrum analyzer (OSA)), and the side mode suppression ratios (SMSRs) are over 35 dB, at maximum power. Meanwhile the FWHMs of the type 3 and type 4 device are more than 0.1 nm and the SMSRs are smaller than 10 dB with multiple intensity peaks. We can find that the type 1 and type 2 devices can operate with single fundamental mode, and the type 3 and type 4 devices operate in multimode, when the oxide aperture diameter is 8 μm. Compared with the type 2 PhC-VCSELs, the type 1 PhC-VCSELs can work at single fundamental mode with lower threshold current.

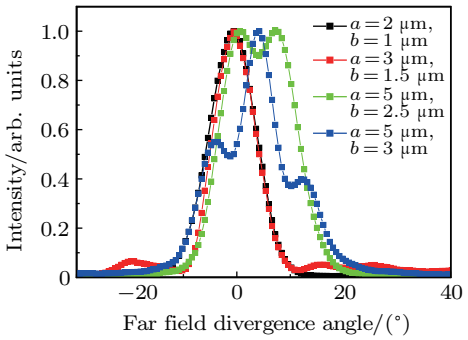


Fig. 4. (color online) Beam profiles of the fabricated PhC-VCSELs measured at maximum output power.

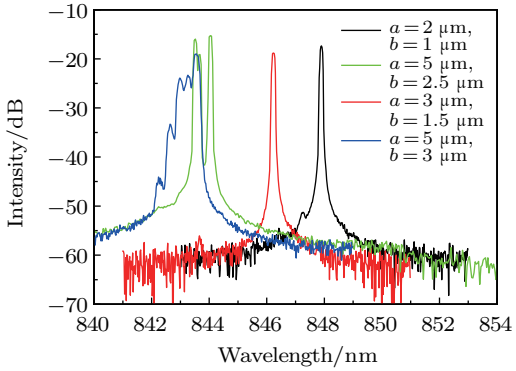


Fig. 5. (color online) Optical spectra of the fabricated PhC-VCSELs measured at maximum output power.

In order to analyze the experimental results, the 3D-FDTD method was used to analyze the produced devices' mode characteristics. Table 3 depicts the Q factors of the cavity modes in the fabricated PhC-VCSELs. We can find that the 0^{th} (fundamental mode) mode Q factor of the type 1 PhC-VCSELs is 2228.98 and the 1^{st} mode Q factor of the devices is 1788.75. From Eq. (2), we can find that the mode loss coefficient of the 0^{th} mode is 17.94 cm^{-1}, while that of the 1^{th} mode is 22.36 cm^{-1} (where $n_{eq} = 3.4$, $\lambda_c = 850$ nm). We can also conclude that the loss difference between the fundamental mode and the high-order modes is high enough to restrict the high-order modes from lasing. The same phenomenon occurred in the type 2 ($a = 3$ μm, $b = 1.5$ μm) PhC-VCSELs cavity. Meanwhile, the fundamental mode Q factor of the type 1 PhC-VCSELs is higher than that of the type 2 PhC-VCSELs

by 320. From Eq. (2), we can find that the fundamental mode loss coefficient of the type 2 PhC-VCSELs is 20.97 cm^{-1}, about 15% larger than that of the seven-point-defect PhC-VCSELs. The high fundamental loss leads to a higher threshold current of the one-point-defect PhC-VCSELs, which was also experimentally demonstrated in Refs. [11] and [33]. For the lattice constant $a = 5$ μm PhC-VCSELs, the mode losses for the fundamental and the high-order modes are nearly the same, so it is possible that the high-order modes can exist simultaneously, and it is difficult for the VCSEL to operate with single fundamental mode.

Table 3. The Q factor of the PhC-VCSELs with different PhC structures.

Structure	0th mode	1st mode	2nd mode
Type 1	2228.98	1788.75	746.101
Type 2	1908.78	1458.33	745.914
Type 3	2214.06	2228.5	2135.1
Type 4	2228.91	2236.33	1911.11

To further analyze the fundamental mode and the high-order mode confinement characteristics of the type 1 and type 2 photonic crystal structures, the transverse mode intensity distributions in the cavities of the type 1 and type 2 devices were calculated and shown in Fig. 6 on logarithmic color scale. For the devices with type 1 photonic crystal structure, the fundamental mode light energy escapes into the air-hole rings of the photonic crystal. However, the seven-point-defect devices fundamental mode light energy is still confined in the emission aperture mostly. The fundamental mode Q factor difference of the two structures originates from the different optical field confinement abilities by the photonic crystal.

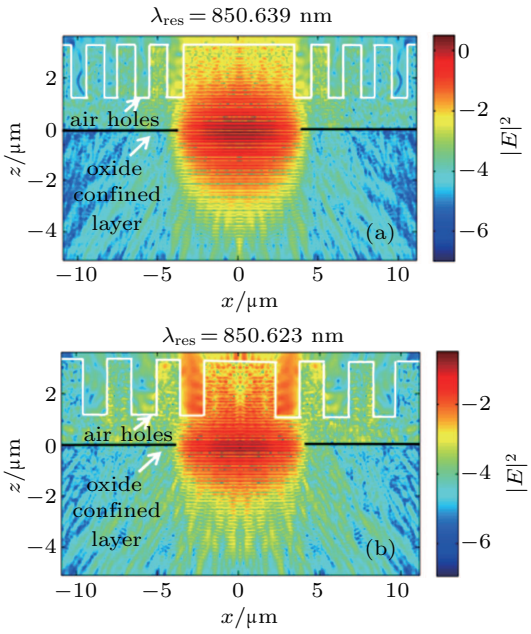


Fig. 6. (color online) Calculated mode intensity profiles of PhC-VCSELs with 8-μm oxide aperture diameter and different photonic crystal structures on logarithmic color scale: (a) the fundamental modes with seven-point-defect PhC structure, (b) the fundamental mode with single-point-defect PhC structure.

According to the experimental and theoretical results, we can find that with the oxide aperture diameter reducing, the performance of the device with the seven-point-defect structure is obviously superior to that of the device with the single-point-defect structure. Therefore, in the following section, the seven-point-defect structure was considered to find the optimal oxide aperture diameter experimentally.

3.2. Mode loss analysis with various oxide aperture diameters

In PhC-VCSELs, when the oxide aperture diameter is reduced to a comparable dimension as the light emission aperture, the oxide aperture would start to affect the mode loss and the mode field distribution. Therefore the transverse mode distribution and mode loss of the VCSEL will now be confined not only by the photonic crystal structure, but also by the oxide aperture. The losses of the high-order transverse modes introduced by the photonic crystal air holes would also be modified by the oxide aperture. In order to analyze the laser cavity resonance modes confined by both the seven-point-defect photonic crystal and the oxide aperture, we simulated the mode loss and mode field distribution as oxide aperture diameter varying from 6 μm to 15 μm. Figure 7 shows the Q factors of the resonance modes with different oxide apertures. According to the figure, we can find when the oxide aperture diameter D is close to or smaller than the emission aperture diameter d (7 μm),the mode losses for the fundamental and the high-order modes are nearly the same, so it is possible that the high-order modes can exist simultaneously and it is difficult for the VCSEL to operate with single fundamental mode. According to the previous simulation results and experimental results of the 8 μm oxide-confined seven-point-defect PhC-VCSELs, the mode loss difference between the fundamental mode and the higher order modes is high enough for the VCSELs to operate with single transverse mode. As the oxide aperture diameter increases, the high-order mode losses quickly increase, while the fundamental mode loss remains unchanged. When the oxide aperture increases to 15 μm, the high-order mode losses of the devices tend to unchangeable. The mode loss difference between the fundamental mode and the high-order modes has the maximum value. At this point, the high-order modes have the largest mode loss and the oxide aperture is much larger than the emission aperture. Thus the optical confinement is provided almost by the photonic crystal. When the oxide aperture diameter is large enough, the stable SFM operation can be realized from suitable photonic crystal structures. The mode properties can be analyzed by the effective index model of the photonic crystal fiber.

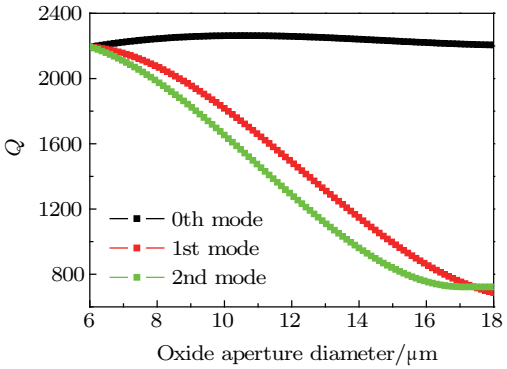


Fig. 7. (color online) The Q factors of the fundamental mode and the high-order modes with different oxide aperture diameters calculated with full 3D FDTD method.

Figure 8 shows the mode intensity profiles in logarithmic color scale for comparison of PhC-VCSELs with different oxide aperture diameters. When the oxide aperture diameter is 6 μm, both the fundamental mode and the high-order mode are well confined in the emission aperture. There is less scattering loss by the air holes of the photonic crystal for all the cavity modes. When the oxide aperture diameter is extended to 10 μm shown in Figs. 8(c) and 8(d), the high-order modes' light energy escapes into the air-hole rings of the photonic crystal, while the fundamental mode is still confined in the emission aperture, indicating the possibility of stable SFM working of the device. When the oxide aperture diameter is extended to 22 μm, the device optical characteristics are not affected by the oxide aperture structure as shown in Figs. 8(e) and 8(f). From Figs. 8(c) and 8(e), we can find that the devices with oxide aperture diameters of 10 μm and 22 μm have the same fundamental mode distributions, revealing nearly the same mode losses. It agrees well with the simulation results of Fig. 7. In contrast to the fundamental mode, the high-order modes distribution of the oxide aperture diameter 22 μm devices is different from that of the oxide aperture diameter 10 μm devices, as shown in Figs. 8(d) and 8(f). We can find that almost all of the photonic crystal air holes are filled with the high-order modes light energy. Accordingly, the devices with oxide aperture diameter 22 μm have the largest high-order mode losses. From the simulation results, it is evident that the photonic crystal structure stabilizes the lateral mode confinement of the VCSEL through introducing selective mode loss of the higher order modes in the oxide confined PhC-VCSELs. Small oxide aperture can reduce the scattering loss of the air holes, and

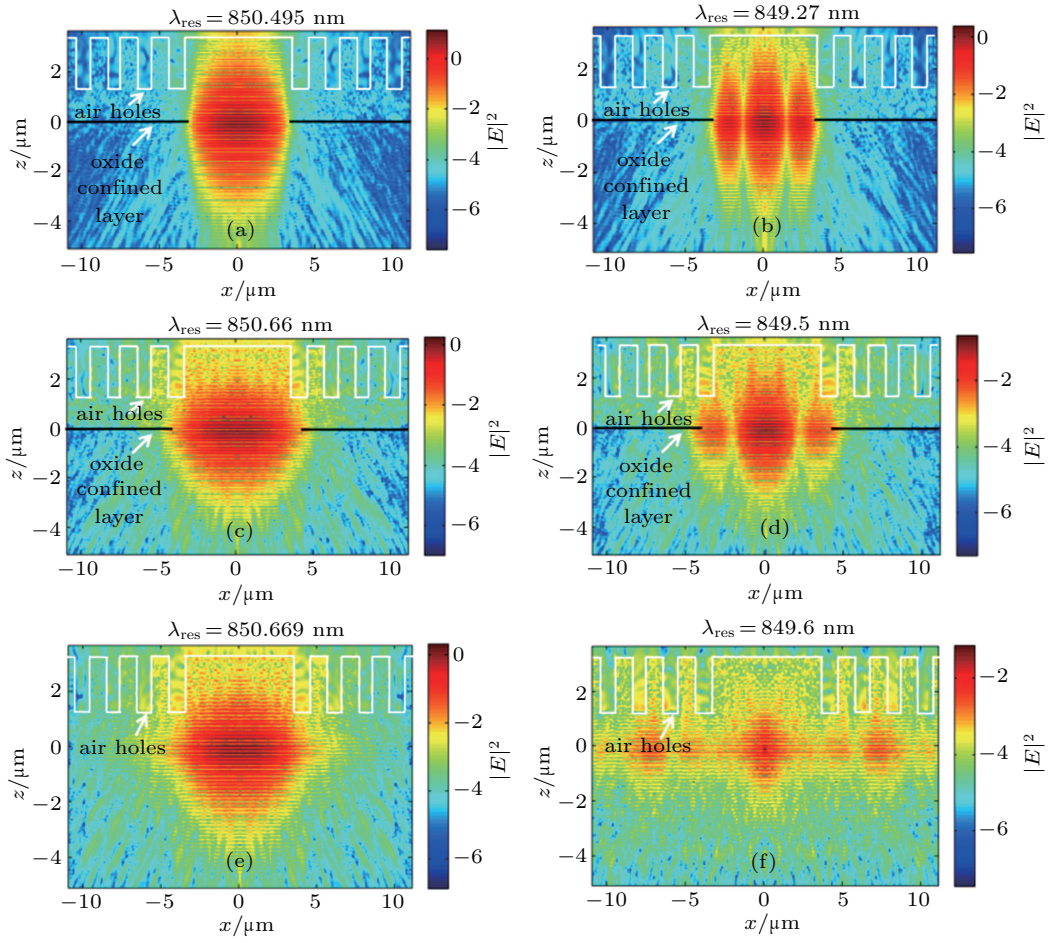


Fig. 8. (color online) Calculated mode intensity profiles of PhC-VCSELs with different PhC structure parameters on logarithmic color scale: (a) the fundamental and (b) the high-order modes with 6 μm oxide aperture diameter, (c) the fundamental and (d) the high-order modes with 10 μm oxide aperture diameter, and (e) the fundamental and (f) the high-order modes with 22 μm oxide aperture structure. White lines indicate the contours of the etched holes and the black lines show the oxide layer of the fabricated PhC-VCSELs.

smaller portion of the light leaves the cavity through the etched holes. The low scattering loss also has the advantage to obtain low threshold currents in oxide-confined PhC-VCSELs. Therefore, optimizing the oxide aperture in PhC-VCSELs can make the device operate at low threshold current and maintain high single fundamental mode output.

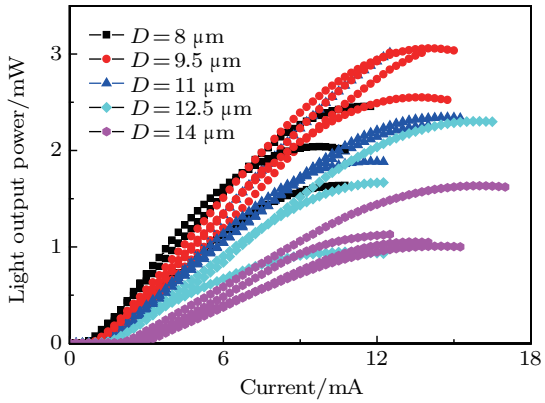


Fig. 9. (color online) CW *L–I* characteristics of the fabricated SFM PhC-VCSELs with different oxide apertures. Devices with the same photonic crystal structure: lattice constant of 2 μm, air hole diameter of 1 μm, and the seven-point-defect diameter $d = 7$ μm.

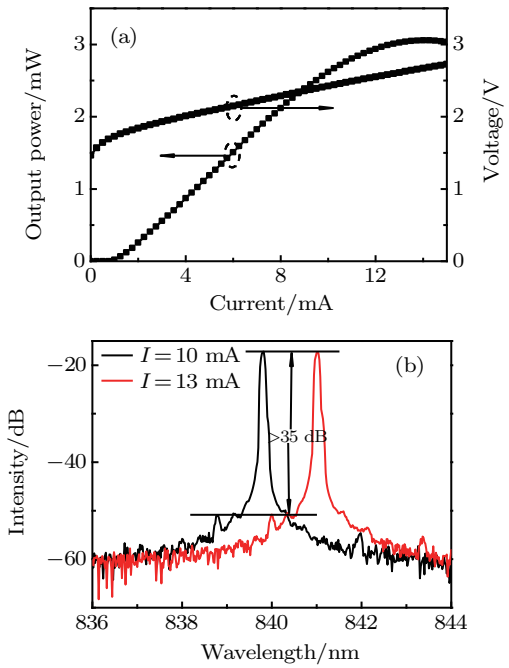


Fig. 10. (color online) (a) Optimized PhC-VCSEL with 10 μm oxide aperture operating in single fundamental mode with 3.1 mW output power. (b) The spectral characteristics of the optimized SFM PhC-VCSELs at maximum output power. Over 35 dB side suppression is maintained.

Figure 9 shows the RTCW *L–I* characteristics of the fabricated seven-point-defect PhC-VCSELs with different oxide aperture diameters. All of the devices work in single mode operation, the divergence angles are less than 10°, the FWHMs are less than 0.1 nm, and the optical spectral SMSRs are over 35 dB. From Fig. 9, we can find that the threshold current of the single fundamental mode VCSELs is closely related to the oxide aperture diameter. To obtain high output power and low threshold current VCSELs devices with single fundamental mode, the oxide aperture diameter ranging from 8 μm to 10 μm is a suitable choice for matching the seven-point-defect PhC-VCSELs light emission aperture.

The optimized experiment result is shown in Fig. 10. The maximum output power of the device is 3.1 mW and the threshold current of the device is 0.9 mA. The optical spectral SMSRs are over 35 dB. The experimental results show that the threshold current of the PhC-VCSELs is reduced by shrinking the oxide aperture. SFM PhC-VCSELs with high output power have been obtained with the optimum control of the oxide aperture diameters and the emission aperture size.

4. Conclusion

The 3D FDTD method was applied to analyze the mode loss in PhC-VCSELs. It was testified as a useful and reliable way to optimize the characteristics of PhC-VCSELs. The transverse mode loss of PhC-VCSELs was highly dependent on both the oxide aperture diameter and the photonic crystal structure. When the fundamental mode loss was reduced and the proper high-order mode dissipation was provided, PhC-VCSELs can work with high output power and low-threshold-current operation. It was experimentally and theoretically demonstrated that the seven-point-defect photonic crystal structure can introduce sufficient high-order-mode loss and less fundamental mode loss in the VCSELs than the single-point-defect one. For the seven-point-defect PhC-VCSELs, the oxide aperture diameter was optimized to improve the characteristics of the PhC-VCSELs, and 3.1 mW single fundamental mode output power and 0.9 mA threshold current were achieved. All these analyses and results show that the seven-point-defect photonic crystal structure and the optimum matching between the photonic crystal emitting aperture and the oxide aperture are essential issues for greatly improving the characteristics of VCSELs.

Acknowledgment

The authors appreciated discussion with Professor Chen Ji and Professor Yong-Zhen Huang.

References

[1] Iga K 2000 *IEEE J. Sel. Topics Quantum Electron.* **6** 1201
[2] Larsson A 2011 *IEEE J. Sel. Top. Quantum Electron.* **1077-260X** 1
[3] Jung C, Jäger R, Grabherr M, Schnitzer P, Michalzik R, Weigl B, Müller S and Ebeling K J 1997 *Electron. Lett.* **33** 1790
[4] Wang W J, Li C, Zhou H Y, Wu H, Luan X X, Shi L and Guo X 2015 *Chin. Phys. B* **24** 024209
[5] Guan B L, Liu X, Jiang X W, Liu C and Xu C 2015 *Acta Phys. Sin.* **64** 164203 (in Chinese)
[6] Kroner A, Rinaldi F, Ostermann J M and Michalzik R 2007 *Opt. Commun.* **270** 332

[7] Shi J W, Chen C C, Wu Y S, Guol S H, Kuo C and Yang Y J 2008 *IEEE Photon. Technol. Lett.* **20** 1121

[8] Unold H J, Riedl M C, Mahmoud S W Z, Jäger R and Ebeling K J 2001 *Electron. Lett.* **37** 178

[9] Zhao Z B, Xu C, Xie Y Y, Zhou K, Liu F and Shen G D 2012 *Chin. Phys. B* **21** 034206

[10] Song D S, Kim S H, Park H G, Kim C K and Lee Y H 2002 *Appl. Phys. Lett.* **80** 3901

[11] Danner A J, Raftery J J, Leisher P O and Choquette K D 2006 *Appl. Phys. Lett.* **88** 1114

[12] Chen C, Leisher P O, Kuchta D M, and Choquette K D 2009 *IEEE J. Sel. Top. Quantum Electron* **15** 673

[13] Xie Y Y, Xu C, Kan Q, Wang C X and Chen H D 2013 *Optics & Laser Technology* **50** 130

[14] Xie Y Y, Xu C, Kan Q, Wang C X, Liu Y M, Wang B Q, Chen H D and Shen G D 2010 *Chin. Phys. Lett.* **27** 0242061

[15] Yokouchi N, Danner A J and Choquette K D 2003 *IEEE J. Sel. Top. Quantum Electron.* **9** 1439

[16] Danner A J, Raftery J J Jr, Yokouchi N and Choquette K D 2004 *Appl. Phys. Lett.* **84** 1031

[17] Xie Y Y, Xu C, Kan Q, Xun M, Xu K and Chen H D 2015 *Opt. Mater. Express* **5** 1998

[18] Yokouchi N, Danner A J and Choquette K D 2003 *Appl. Phys. Lett.* **82** 3608

[19] Yang H P D, Lai F I, Chang Y H, Yu H C, Sung C P, Kuo H C, Wang S C, Lin S Y and Chi J Y 2005 *Electron. Lett.* **41** 326

[20] Leisher P O, Danner A J and Choquette K D 2006 *IEEE Photon. Technol. Lett.* **18** 2156

[21] Yokouchi N, Danner A J and Choquette K D 2003 *Appl. Phys. Lett.* **82** 1344

[22] Alias M S and Shaari S 2010 *Appl. Phys. B* **100** 4340

[23] Danner A J, Raftery J J, Kim T and Leisher P O 2005 *IEICE Trans. Electron.* **E88-C 5** 944

[24] Liu A, Xing M, Qu H, Chen W, Zhou W and Zheng W 2009 *Appl. Phys. Lett.* **94** 1911051

[25] Cao T, Xu C, Xie Y Y, Kan Q, Wei S M, Mao M M and Chen H D 2013 *Chin. Phys. B* **22** 024205

[26] Xie Y Y, Kan Q, Xu C, Zhu Y X, Wang C X and Chen H D 2012 *IEEE Photon. Technol. Lett.* **24** 464

[27] Alias M S and Shaari S 2010 *IEEE J. Lightw. Technol.* **28** 1556

[28] Alias M S, Shaari S, Leisher P O and Choquette K D 2010 *Appl. Phys. B* **100** 453

[29] Dems M, Chung I S, Nyakas P, Bischoff S and Panajotov K 2010 *Opt. Express* **18** 16042

[30] Jo D H, Vu N H, Kim J T and Hwang I K 2011 *Opt. Express* **19** 18272

[31] Park H G, Hwang J K, Huh J, Ryu H Y, Kim S H, Kim J S and Lee Y H 2002 *IEEE J. Quantum Electron.* **38** 1353

[32] Zhang Y, Khan M, Huang Y, Ryou J, Deotare P, Dupuis R and Lončar M 2010 *Appl. Phys. Lett.* **97** 0511041

[33] Nyakas P 2007 *IEEE J. Lightw. Technol.* **25** 2427

[34] Czyszanowski T 2010 *Opto.Electron. Rev.* **18** 56

[35] Czyszanowski T, Dems M, Sarzała R P, Nakwaski W and Panajotov K 2011 *IEEE J. Quantum Electron.* **47** 1291

[36] Siriani D F, Leisher P O and Choquette K D 2009 *IEEE J. Quantum Electron.* **45** 762

[37] Czyszanowski T, Dems M, Thienpont H and Panajotov K 2007 *Opt. Express* **15** 1301

[38] Gehrsitz S, Reinhart F K, Gourgon C, Herres N, Vonlanthen A and Sigg H 2000 *J. Appl. Phys.* **87** 7825

[39] Adachi S 1982 *J. Appl. Phys.* **53** 5863